Proceedings of the Combustion Institute, Volume 29, 2002/pp. 909–916

DEVELOPMENT OF A MICROREACTOR AS A THERMAL SOURCE FOR MICROELECTROMECHANICAL SYSTEMS POWER GENERATION

J. VICAN,[1] B. F. GAJDECZKO,[1] F. L. DRYER,[1] D. L. MILIUS,[2] I. A. AKSAY[2] AND R. A. YETTER[3]

[1]*Department of Mechanical and Aerospace Engineering*
[2]*Department of Chemical Engineering*
Princeton University
Princeton, NJ 08544, USA
[3]*Department of Mechanical and Nuclear Engineering*
Propulsion Engineering and Research Center
The Pennsylvania State University
University Park, PA 16802, USA

An alumina ceramic 12.5 × 12.5 × 5.0 mm microreactor was constructed using a modified stereolithography process. The design was based on a "Swiss roll" concept of double spiral-shaped channels to facilitate a high level of heat transfer between the reactants and combustion products and wall surface contact of the flow through the microreactor body. Self-sustained combustion of hydrogen and air mixtures was demonstrated over a wide range of fuel/air mixtures and flow rates for equivalence ratios from 0.2 to 1.0 and chemical energy inputs from 2 to 16 W. Depositing platinum on gamma alumina on the internal walls enabled catalytic ignition at or near room temperature and self-sustained operation at temperatures to 300 °C. Catalyst degradation was observed at higher operating temperatures and reignition capabilities were lost. However, sustained operation could be obtained at wall temperatures in excess of 300 °C, apparently stabilized by a combination of surface and gas-phase reaction phenomena. A global energy balance model was developed to analyze overall reactor performance characteristics. The reactor design and operating temperature range have potential applications as a heat source for thermoelectric and pyroelectric power generation at small scales compatible with microelectromechanical systems applications.

Introduction

With the successful development of microelectromechanical systems (MEMS) devices such as microsensors and actuators, there has been considerable interest in developing chemically fueled micropower generation systems that could produce 300 mW or less, with footprints sufficiently small to colocate communications, sensors, actuators, and power systems all on the same chip. Chip level integration that includes power generation would eliminate interconnects and benefits applications involving multipoint distributed sensing, communications, and response. Depending on the battery technology assessment source [1,2], liquid hydrocarbons are from 12 to more than 50 times more energy-dense (by volume) than advanced electrochemical sources, provided that ambient air is available as the oxidizing agent. Thus, overall conversion efficiencies to equivalent electrical output as low as 10% would suggest chemical energy conversion could be preferred in terms of useful life.

Conventional gasoline or diesel fuels are not likely to be useable in MEMS chemical conversion systems, because of fuel chemical instability (property degradation) in long-term storage, resulting in particulates and deposits. However, liquefied gaseous fuels (propane, butane, and their conjugate olefins) or hydrocarbon liquids designed specifically for long shelf life (and even higher energy densities) are reasonable candidates for MEMS chemical energy conversion devices. Chemically driven power-generation modes may also be advantageous for specific applications such as complementing battery sources for high-power output or power peaking.

A myriad of chemical-to-electrical conversion approaches are, in principal, open to consideration at the MEMS level. Current research efforts using mechanical motion to generate power include micro-gas turbines, micro-Wankel engines, and linear, micropulsating systems based on oscillating electrical field and piezoelectric deflections/oscillations [3]. Direct energy conversion concepts without moving parts that are being considered include fuel cells and thermal reactors coupled to thermoelectric, photovoltaic, and pyroelectric devices. Highly efficient fuel cells presently operate only on pure hydrogen. However, hydrogen storage technologies producing volumetric energy densities approaching liquefied gaseous fuels do not yet exist. On-board hydrogen

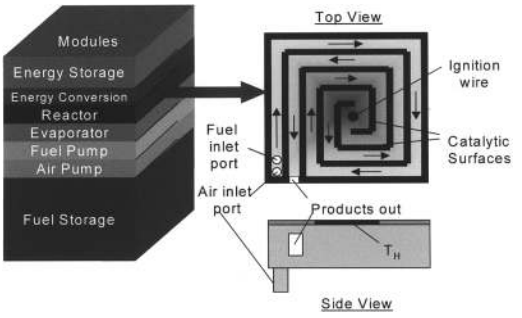

FIG. 1. A conceptual power supply with an excess enthalpy ("Swiss roll") catalytic reactor.

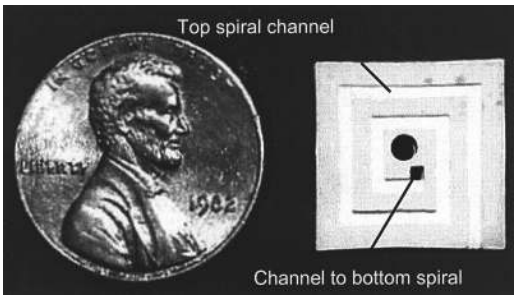

FIG. 2. Cross-section of exemplar microreactor design fabricated by stereolithography. Top flow channel (same on bottom) is visible, spiraling into the center of the structure.

generation significantly increases the complexity of the system, and as a result, may eliminate the overall system efficiency advantage and negatively affect reliability and operating lifetime.

Thermal microreactors of various types, used with direct thermal to electrical energy conversion or coupled with external heat engine concepts offer the advantages of simplicity, longer-term compatibility with various hydrocarbon fuel types, and flexibility in decoupling system chemical conversion and energy extraction time scales. Of primary importance to these concepts is a chemical to thermal energy conversion reservoir coupled to methodologies to convert thermal to electrical energy (Fig. 1). Along with us, other groups, for example, Ref. [4], are developing thermal microreactor designs based on the concept of excess enthalpy combustion [5]. As a result of regeneratively preheating the reactants, combustor temperatures can achieve super adiabatic temperatures, increasing combustor efficiency, extending fuel/air mixture limits for which gas-phase kinetics remain explosively chain branched, and reducing wall quenching.

Since 1998, we have been developing thermal microreactors on small scales that would achieve operating temperatures below 1100 K that could eventually incorporate excess enthalpy operating principles, that are compatible with eventual use of liquefied gaseous hydrocarbons as fuels, and that have potential for being scaled to even smaller dimensions. The microreactor design described in this paper (see Fig. 2) is intended to provide a favorable environment for microscale combustion of gaseous fuel and air mixtures. A layer of catalyst (platinum) is deposited on the internal walls of the channels to lower the range of the operating temperatures. The spiral "Swiss roll" design shown provides a number of desirable features, including: (1) thermal energy transfer mechanism to preheat the reactants using the exhaust heat combustion volume, (2) relatively large internal surface/volume ratio needed for the heat transfer through the walls and for effective action of the catalyst, and (3) large top- and bottom-face surface area for the heat transfer to external devices.

In the present paper, we describe the reactor and the fabrication process, develop an analytical model to characterize the performance of the reactor, and present results on the operation of the reactor with mixtures of hydrogen and air. In addition, the reactor is coupled to commercial thermoelectric modules to demonstrate chemical to electrical energy conversion at the length scales of the present reactor. Advancements in reducing the scale of the reactor, improving heat management, and implementing hydrocarbon fuels will be discussed in forthcoming papers.

Microreactor Fabrication

Three-dimensional stereolithography was utilized to manufacture the microreactors. A three-dimensional virtual solid body produced by computer-aided design is "sliced" finely (0.075 mm) along the Z-axis, creating a build file consisting of a stack of *X–Y* layers. During the build, sublayers are successively added to the part by raster scanning an UV laser across its *X–Y* surface, wetted by a photocurable bath of liquid resin [6]. The photocured, solidified layer is moved down by one layer thickness inside the liquid bath, and the patterned curing process is repeated. The resin used is a highly concentrated colloidal dispersion prepared by dispersing alumina powder in an aqueous solution of ultraviolet curable polymers. The ceramic green body manufactured is subsequently dried, the photocurable binder is burned out, and the part is sintered to full density.

The ceramic microreactor part (Figs. 2 and 3) can be generated in about 4 hr and is an alumina monolith with two distinct approximately 800 μm^2 channels (one each side) that spiral inward, joining near the center of the body. The approximate length of the internal path was 0.1 m. A larger central hole is added to the structure to accommodate the positioning of an electrical resistance heating wire

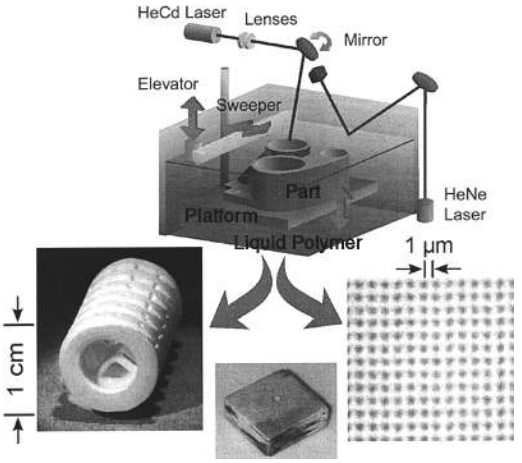

FIG. 3. Stereolithography process with examples of fabricated parts. The finished reactor, showing inlet and outlet holes on the front surface, is shown in the center.

through the center of the body to provide sufficient heat to initiate catalytic reactions of a premixed fuel/air mixture flowing through the spiral passages.

Following stereolithographic fabrication, the entrained liquids are removed from the unsintered part (green body) and the polymers are burned out of the structure at low temperatures using a stepwise heating program raising the part temperature to 425 °C over 6 hr. The green body is then sintered at high temperatures (1550 °C for 2 hr) to full density. Postsintering processing includes the addition of a platinum catalyst supported on a gamma alumina wash coat deposited within the microreactor channels. The catalyst is added by injecting hydrogen hexachloroplatinate into the channels and heating the dried microreactor to 350 °C for 2 hr in air and then for 8 hr in hydrogen.

Microreactor Model Analysis

As a prelude to detailed computational fluid dynamics and thermal stress analyses, a simple energy balance model was utilized to characterize overall operational characteristics of an uninsulated reactor in a quiescent environment. Lumped heat capacitance was assumed since Biot numbers for the structure are estimated to vary from 0.001 to 0.1, depending upon their definition. The Biot number was defined in several ways so that a range of Biot numbers was obtained. The external heat transfer coefficient was compared to the overall internal heat transfer coefficient (which included convective heat transfer across the channels in the reactor body). Biot numbers were also calculated using the classical definition for the internal conduction heat transfer rate to the external heat transfer. The chemical reaction was also assumed to be complete within the reactor; this assumption can be globally removed using experimental measurements of the actual chemical conversion efficiency. Thermal dissociation of products was assumed negligible and the chemistry was described by a single overall global reaction. At such low Biot numbers and the heat recovery nature of the "Swiss roll" design, the reactor body and internal gas temperatures were assumed equal and uniform in the model. The lumped heat capacitance assumption is verified below from thermocouple measurements at various locations on the external surface. Under these assumptions and steady-state conditions, the energy balance is

$$\dot{m}\overline{c_{p,r}}T_i + \dot{m}Q_{rp} - \dot{m}\overline{c_{p,p}}T_s - \bar{h}A(T_s - T_\infty) - \sigma\epsilon A(T_s^4 - T_\infty^4) = 0$$

where $\dot{m}$ is the mass flow rate of fuel and oxidizer, $\overline{c_{p,r}}$ is the reactant mixture specific heat, $\overline{c_{p,p}}$ is the product mixture specific heat, Q_{rp} is the lower heat of combustion per unit mixture mass, T_i is the inlet temperature of the reactants, T_s is the reactor body and exhaust product temperature, T_∞ is the environmental temperature, h is the film coefficient, A is the reactor surface area, σ is the Stefan-Boltzmann constant, and ϵ is the reactor body emissivity. Thermodynamic data were obtained from the JANNAF tables, the film coefficient was estimated from the Nusselt number correlation of Churchill and Chu [7] for a flat vertical surface and Ra_L numbers less than 10^9, and ϵ of aluminum oxide was assumed equal to 0.69 [8] independent of temperature. The above equation was solved for the surface temperature, which is compared to experimental measurements below. Note that as long as heat transfer between the channels and the reactor body remain high, the model places no restriction on where the heat release occurs (surface catalysis or homogeneously in the gas phase). Reaction quenching at the surface is not an issue, as long as energy transfer to and from the surface maintains the surface temperature above the gas-phase explosion limit.

Figure 4 shows the predicted reactor surface (body) temperature (T_s) and gas residence times (τ) as a function of equivalence ratio, ϕ, for a fixed total volume flow rate of reactants of 80 cm^3/min. Volumetric flow rates are reported for standard conditions (298 K, 1 atm). Predicted surface temperatures vary from approximately 350 to 530 K for variations in ϕ from 0.1 to 1, while residence times decrease from about 68 to 52 ms. Predicted residence times exceed the estimate for mass diffusion times to the walls by at least a factor of 50, indicating sufficient mass turnover for complete reaction. Body temperatures below ~373 K may initiate water condensation on the reactor channel surfaces. Thus, for the present reactor, the minimum ϕ for 80 cm^3/min flow rate is anticipated to be 0.2.

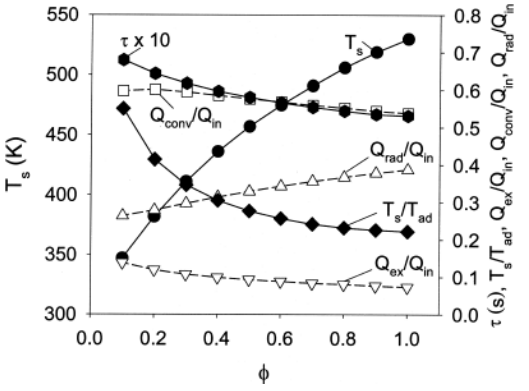

FIG. 4. Predicted reactor temperature, residence time, energy loss distributions, and thermal efficiency for a total volumetric flow rate of 80 cm^3/min.

The distributions of heat loss by convection at the surface, Q_{conv}, heat loss by radiation, Q_{rad}, and unrecovered energy in the exhaust, all relative to the heat input, Q_{in}, are also shown in Fig. 4. At $\phi = 0.1$, ~60% of the energy loss occurs by convection, 26% occurs by radiation, and the remaining 14% is retained in the exhaust gases. At $\phi = 1.0$, energy loss by convection accounts for ~54% of the energy input, radiative loss accounts for ~39%, and the exhaust contains ~7% of the added energy. Also shown in Fig. 4 is the ratio of the reactor temperature to the adiabatic flame temperature that the body would assume if both radiation and convection losses were eliminated. The adiabatic flame temperature was calculated using the CEA code [9] and therefore includes dissociation of product species. In the reactor's present operation and configuration, this ratio is an indication of the thermal efficiency. At constant total flow rate, leaner mixtures result in reduced operating temperatures and, consequently, less heat loss and better efficiencies. However, leaner mixtures also imply less power input. For a variation in ϕ at constant input power (i.e., constant fuel flow rate), the results are similar to those presented for constant total mass flow rate. However, as ϕ is decreased, the total air mass flow rate becomes significant, decreasing the residence times in the reactor substantially. Short residence times decrease the percentage of heat loss by convection and radiation, and the majority of the input energy now remains in the exhaust gas. Thermal efficiencies as indicated by T_s/T_{ad} are also higher obtaining a value of 72% at $\phi = 0.1$.

The high thermal efficiencies observed at low ϕ, however, come with a tradeoff. In a complete system, such high mass flow rates will require more energy for pumping power, and therefore, the net gains of running extremely lean are not obvious from a systems point of view. Furthermore, short residence times may not be sufficient to obtain complete reaction in the reactor. Optimization of the above parameters will depend on the specific fuel, and its chemical oxidation times, whether they be catalytically produced or principally controlled by gas-phase oxidation chemistry. As a result of the very nature of the present configuration and size of the reactor, it does not operate in the excess enthalpy mode as described above. In such a system, temperature gradients would need to be maintained across the reactor, in contrast to the low Biot number system studied here. Future work is needed to isolate reactor temperature to achieve such gradients at small scales. One simple methodology is by combination of several layers of "thin-sheet" layers of similar design to this reactor, with thermoelectric films sandwiched between the successive layers of the composite.

Microreactor Experiments

Experiments were performed in a temperature-controlled laboratory (25.5 ± 1 °C) for comparison with the simple theory above. Hydrogen was used as the fuel because of its catalytic reaction characteristics on platinum/gamma alumina catalysts. Hydrogen and air were supplied from pressurized cylinders with pressure regulators and a needle valve in each line to induce the sonic discharge condition for flow control. Flow rates were determined using soap bubble meter measurements of each individual flow. The streams were then mixed and delivered to the microreactor through a 5 cm long section of No. 24 stainless-steel hypodermic tubing mated to the ceramic microreactor body. An identical arrangement transferred exhaust from the microreactor to composition measurement equipment downstream of the reactor. The alumina reactor was interfaced with supply and exhaust tubes using glass welds. The exhaust is immediately cooled by passing the gases through an ice bath that also removes water from the flow to a defined absolute humidity. The cooled gases are then diluted by known amounts of dry nitrogen such that the oxygen remaining in the stream will be in a concentration range that can be measured using a Delta F trace oxygen analyzer. Net oxygen consumption was determined to evaluate the chemical conversion efficiency within the microreactor. Nickel-chromium/nickel-aluminum (Type K) and nickel-chromium/copper-nickel (Type E) thermocouples with junction diameters of approximately 25 μm were affixed to the microreactor using thermally conductive, low-expansion ceramic cement. Thermocouples were located on the face center and in the middle of each of the two sides of the reactor adjacent to the exhaust/intake port location at one of the reactor corners. Measured temperature differences were generally within ±1.5 °C during steady-state operation (even at maximum operating

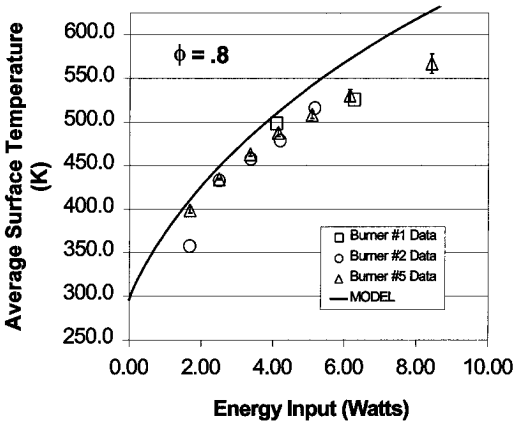

FIG. 5. Experimental microreactor temperature (symbols) as a function of input power for three different reactors at an equivalence ratio of 0.8. Line is the model prediction.

temperature), experimentally confirming that the operating reactor was at uniform temperature. Experiments were performed to define the range of operating parameters over which self-sustained reaction could be accomplished without jeopardizing mechanical integrity of the reactor (through excessive operating pressure and temperature). Hydrogen and air flow rates, as well as the steady-state operating temperature of the reactor, were monitored during the experiments.

Two types of initiation assistance were employed. For experiments at operating temperatures less than 300 °C, the microreactors were enclosed in a Lindberg clamshell oven, and the monitored oven temperature was adjusted using a Vari-AC voltage manual adjustment of oven power until reaction initiation was noted by microreactor temperatures beginning to exceed oven temperature. Once reaction was stabilized, the oven was turned off and opened, and the reactor reached the reported equilibrium operating temperatures in open ambient air. In a second series of experiments, which investigated operating temperatures higher than 300 °C, the microreactor as shown in Fig. 2 was equipped with a Kanthal wire heater mounted in the center reactor hole using thermally conducting ceramic cement. A small micro-oven was equipped with terminals for the heating wire, routed through the small hole in the center of the microreactor. The heating wire was powered with AC current through an adjustable autotransformer.

Pressure drop across the reactor was measured as a function of air flow rate. In non-reacting experiments, the reactor was heated to 300 °C in the Lindberg clamshell oven and air was passed through the reactor. At a flow rate of 25 cm^3/min, a pressure drop of 6.9 $\times$ 10^3 N-m^{-2} was measured, while at a flow rate of 210 cm^3/min, a pressure drop of 9.65 $\times$ 10^4 N-m^{-2} was obtained. Most of the pressure drop is a result of the flow through the No. 24 hypodermic tubing, which had an internal diameter of approximately 350 μm. For these flow rates, the pressure drop is equivalent to a pumping power requirement of approximately 2.8 to 330 mW. As discussed above, lean mixtures and high power may have significant pumping losses.

Two operating regimes became apparent as experiments proceeded. Autoinitiation could only be achieved with microreactors that had not experienced operating temperatures above about 300 °C. For equilibrium operating conditions below this temperature boundary, the reaction of H_2 and O_2 cannot occur homogeneously in the gas phase within the available reaction residence times, and the reaction must proceed entirely by surface catalysis. However, extensive testing of the catalyst materials and procedures used (deposited in heated ceramic tubes) clearly identifies that the catalyst and support structure are degraded by exposure to operating temperatures in excess of 300 °C. Without the presence of other stabilizers, the gamma alumina substrate reverts to alpha alumina form and the distributed area of the platinum catalyst itself is reduced by sintering and agglomeration of the distributed platinum catalyst [10]. These observations are consistent with literature data. We found that if microreactors had been exposed to operating temperatures much in excess of 300 °C, room temperature autoinitiation could no longer be obtained. We also noted that catalytic chemical conversion efficiency at lower temperatures was irreversibly degraded. At operating temperatures higher than 300 °C, the reaction is apparently sustained within the reactor as a result of both gas-phase chemistry, as well as interactions at the microreactor surface. These results are consistent with published spontaneous ignition temperatures (400 °C) of H_2/air mixtures [11]. Such empirical measurements are, however, strongly affected by surface material considerations and surface to volume ratio. Experiments show that some hydrogen conversion can occur on the reactor surfaces at a low temperature even without the presence of catalyst. It is also clear that complete conversion of hydrogen should occur in small passages over some range of higher gas/wall temperatures that exceed that required to achieve the critical branching ratio for chain branched kinetics, inclusive of wall termination effects.

Although the ignition phenomenon was found to be reactor-dependent, steady-state operating characteristics were extremely reproducible. Fig. 5 compares the measured operating temperatures for three reactors as functions of chemical energy input for H_2/air mixtures (ϕ = 0.8). The reproducibility of the experimental measurements is remarkably consistent over a range of power inputs from about

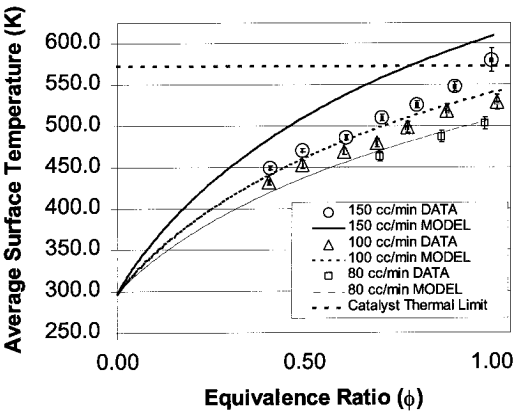

FIG. 6. Experimental microreactor temperature (symbols) as a function of equivalence ratio for three different total reactor flow rates. Lines are model predictions.

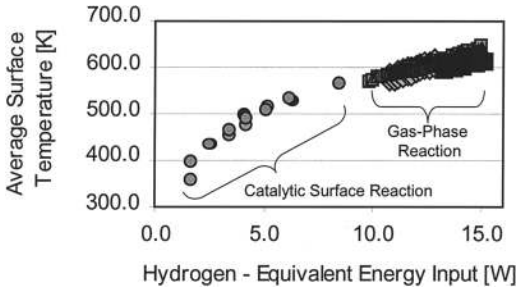

FIG. 7. Body temperatures for high input power operation illustrating regimes dominated by catalytic surface reaction and by combined heterogeneous surface and gas phase chemistry.

2 to 6 W. Below approximately 1.8 W power input, steady-state reactor operation was difficult to achieve. The reactor temperature was observed to oscillate, principally due to water condensation in the reactor channels as a result of microreactor temperatures dropping below the condensation temperature. Once the channel was filled, reactant flow would clear the channel of condensate, permitting reignition.

Comparison of experimental results with modeling results (the lines in Figs. 5 and 6) shows that the model described above overestimates the resulting surface temperature for a given power input. Fig. 6 reports data for three different flow rates of reactive mixture with varied energy input by changing equivalence ratio. While increased flow rate leads to increased energy input, residence time within the reactor is also reduced as discussed above. These results suggest the estimations of heat losses are reasonably accurate and that experimental/model disparities are primarily due to chemical conversion efficiency variations. The larger differences between the modeling results and experiments at high flow rates can be attributed to incomplete conversion as a result of shorter residence times. Catalytic conversion also may be a function of equivalence ratio as noted by the nonlinear behavior of the experimental data for the highest flow rate and equivalence ratio measurements. Measurements of conversion efficiency using the trace oxygen analysis approach confirm these speculations [10]. High-temperature operating characteristics were obtained by operating the reactor under increased input power levels. Higher input powers continue to extrapolate the body temperatures to higher values (Fig. 7).

To demonstrate electrical power generation at the length scales of the present reactor, the microreactor was sandwiched between two commercial thermoelectric modules (Melcor Hot 2.0-31-F2A) and two cold reservoirs. Each thermoelectric module consisted of 31 p- and n-type pairs of doped bismuth-telluride semiconductors connected electrically in series and thermally in parallel. The two modules were connected in series, and power output was measured across a variable potentiometer. Fig. 8 shows that the maximum output power varied from approximately 30 to 55 mW at a load resistance of $\sim 6\ \Omega$ for chemical input powers of 6.8 to 9.1 W. As shown in Table 1, the cold reservoir temperature was maintained at 23 °C, while the hot reservoir temperature increased from ~100 to 115 °C. These temperatures are considerably lower than those shown in Fig. 5 as a result of the increased heat loss across the thermoelectric modules. The resulting conversion efficiency varied from ~0.44 to 0.57%. Considering that the modules were not optimized for the present conditions (e.g., temperature limitations on thermocouple solder connections), plus only 38% of the surface was covered with thermocouples, the present results are promising. The bismuth-telluride modules used here had an upper temperature limit of about 225 °C. Although not yet available commercially, several classes of materials (Si-Ge alloys, doped Pb-Te, the recently discovered Skudderudite alloys based on $CeFe_4Sb_{12}$, and perhaps, transition metal silicides) have potential for thermoelectric constructs with higher figures of merit and increased temperature limits.

Summary

This paper reports a number of important milestones: (1) Self-sustained chemical reaction (with and without catalysis) was demonstrated in small structures; (2) conversion of fuel to electrical power has been demonstrated for commercial thermoelectric systems; (3) micropower generation systems in alumina have been microfabricated using ceramic stereolithography; and (4) some capabilities and critical issues important to the emerging micropower

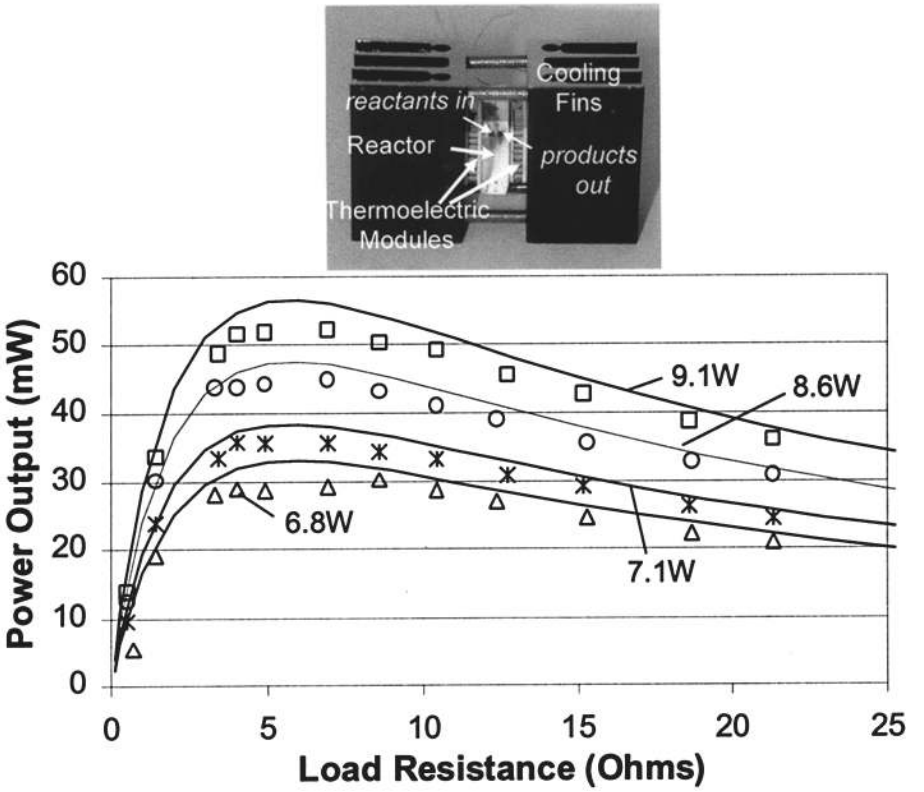

FIG. 8. Power output from commercial thermoelectric modules as a function of load resistance and chemical input power.

TABLE 1
Power generation with coupled micro reactor and commercial thermoelectric (TE) coolers

Chemical power (W)	H_2 flow rate (cc/min)	Total flow rate (cc/min)	ϕ	Open circuit voltage (V)	Maximum power out (mW)	T_{HOT} (°C)	T_{COLD} (°C)	Open circuit ΔT (°C)	η (%)	η_c (%) adjusted for TE-covered surface area
6.83	50.1	148	1.21	0.876	30.1	101.2	23	78.3	0.44	1.2
7.14	146	146	1.01	0.936	35.7	98.5	23	75.5	0.50	1.3
8.59	176	176	1.02	1.041	44.8	108.2	23	85.2	0.52	1.4
9.10	188	188	1.06	1.136	52.2	115.5	23	92.5	0.57	1.5

MEMS knowledge base have been identified and demonstrated.

The present study has shown that because of the small length scales and flow rates involved in the microreactor, a nearly uniform reactor body and gas flow temperature are obtained. In a quiescent environment with an uninsulated reactor, significant heat losses from the surface of the reactor via convection and radiation occur. Methods to reduce heat losses are now under study. However, it should be noted that even if convection losses were minimized through methods such as vacuum insulation, the radiation losses would continue to play a significant role, unless radiation-shielding approaches are pursued. In the present reactor, the catalyst was distributed on the internal channels throughout the reactor body. Future designs are under development to limit catalyst location to the center regions of the reactor, benefiting some of the possible approaches to reducing heat losses.

Acknowledgments

This research was supported by grants from ARO/MURI and DARPA (through subcontract to Dyncorp, Inc.).

REFERENCES

1. Koeneman, P. B., Bush-Vishniac, I. J., and Wood, K. L., *J. MEMS Systems* 6(4):355 (1997).
2. Nowak, R., "*Batteries and Fuel Cells,*" MEMS Based Microscale Power Generation and Energy Conversion Concepts and Systems, DARPA Workshop, Arlington, VA, February 27–28, 1998.
3. Fernandez-Pello, C., *Proc. Combust. Inst.* 29:883–899 (2002).
4. Sitzki, L., Borer, K., Wussow, S., Schuster, E., Maruta, K., and Ronney, P. D., "*Combustion and Power Generation in Microscale Excess Enthalpy Burners,*" paper 111, U.S. Sections Second Joint Meeting of the Combustion Institute, Oakland, CA, March 26–29, 2001.
5. Weinberg, F., *Combust. Sci. Technol.* 121:3 (1996).
6. Garg, R., Prud'homme, R. K., and Aksay, I. A., *J. Opt. Soc. Am. A* 15(4):932 (1998).
7. Churchill, S. W., and Chu, H. H. S., *Int. J. Heat Mass Transfer* 18:1323 (1975).
8. Incropera, F. P., and DeWitt, D. P., *Fundamentals of Heat and Mass Transfer, 4th ed.,* Wiley, New York, 1996.
9. McBride, B. J., and Gordon, S., "Computer Program for Calculation of Complex Equilibrium Compositions and Applications," *NASA reference publication 1311,* Lewis Research Center, Cleveland, OH, 1996.
10. Shinjoh, H., Muraki, H., and Fujitani, Y., in *Studies in Surface Science and Catalysis 71: Catalysis and Automotive Pollution Control II* (A. Cruzq (ed.), Elsevier Science, Amsterdam, 1991, p. 617.
11. Zabetakis, M., U.S. Bureau of Mines Bulletin 627, 1965.
12. Vican, J., *Operational Characterization of a Catalytic Micro-Combustor for MEMS Scale Electrical Power Production,* Fall Independent Work Report, Mechanical and Aerospace Engineering, Princeton University, Princeton, NJ.